RSC Advances

PAPER

View Article Online
View Journal | View Issue

Cite this: *RSC Adv.*, 2020, **10**, 31720

Solution-phase molecular recognition of an azafullerene-quinoline dyad by a face-to-face porphyrin-dimer tweezer†

Anastasios Stergiou, *[a] Aikaterini K. Andreopoulou, [b] Joannis K. Kallitsis[b] and Nikos Tagmatarchis *[a]

Received 7th July 2020
Accepted 10th August 2020

DOI: 10.1039/d0ra06195f

rsc.li/rsc-advances

A face-to-face porphyrin dimer, $(H_2P)_2$ "porphyrin tweezer", was explored as a photo- and redox-responsive host for the molecular recognition of an azafullerene ($C_{59}N$) derivative bearing an amphoteric pentafluoroquinoline (FQ) domain. The intramolecular electronic coupling between the FQ substituent and the $C_{59}N$ cage, within the newly synthesized $C_{59}N$-FQ dyad was evaluated, while the neutral and protonated form of the covalently attached FQ moiety were utilized as recognition motifs for the $(H_2P)_2$ tweezer. Complementary photophysical and electrochemical techniques were applied to investigate the electronic communication between the porphyrin-dimer $(H_2P)_2$ tweezer and the azafullerene cage as mediated by the FQ unit.

Introduction

Azafullerene $C_{59}N$[1,2] is the most explored heterofullerene[3] participating in light harvesting nanoarchitectures.[4] Starting from the parent azafullerene dimer $(C_{59}N)_2$, a series of mono-adducts can be prepared *via* the $C_{59}N^+$ intermediate species.[5] In this respect, several $C_{59}N$-based dyads have been realized by the covalent incorporation of arenes,[6] ferrocene,[7] phthalocyanine,[8] corole,[9] perylene[10] and oligophenylenevinylene[11] derivatives onto the $C_{59}N$ cage. Apart from the mono-adducts, $C_{59}N$ has also a rich chemistry towards multi-addition patterns.[12–17] Notably, we recently reported the tether-directed regioselective synthesis of an equatorial-face bis-adduct of $C_{59}N$, as single isomer, based on a two-step mono-addition reaction sequence employing cyclo-[2]-octylmalonate.[18] In contrast, the supramolecular chemistry of $C_{59}N$ is less explored. Recent advances on the chemistry of carbon nanobelts[19–22] empowered the realization of supramolecular assemblies in solution driven by the molecular recognition of the $C_{59}N$ cage by [10]-cycloparaphenylene ([10]CPP) nanohoops through π–π interactions at the concave–convex interface.[23,24] Furthermore, the shielding of the labile $C_{59}N^{\bullet}$ radical was enabled by supramolecular complexation with [10]CPP rings.[25] In addition, the supramolecular chemistry of functionalized $C_{59}N$ cages is currently limited to derivatives owing monodentate nitrogen ligands suitable for coordination to the metal center of light harvesting molecules such as zinc-phthalocyanines[26] and zinc-porphyrins.[27,28]

Quinolines are amongst heteroatom semiconducting organic species that have gained increased scientific attention due to their easy and versatile synthesis,[29] excellent thermal and mechanical properties, but more importantly due to their interesting photonic, electronic, and conductive characteristics.[30] The reverse protonation on the imino group[31] allows their use as pH tunable sensors,[32,33] while their ability to complex a variety of metal ions or organic conjugates reveals their applicability also as selective fluorescent chemosensors.[34] Moreover, the incorporation of electron withdrawing units onto quinolines allows further modulation of their optical and electronic properties. To this end, the incorporation of a perfluorophenyl group has proven to be a valuable addition onto the quinoline core, since it significantly lowers their LUMO levels. Moreover, the presence of the halogen atoms enabled their straightforward transformation to azides, allowing the direct incorporation on the sp^2 skeleton of carbon nanostructures *via* cycloaddition reactions.[35–37] More specific, (tetrafluoro)azidophenyl-quinolines have been employed for the functionalization of carbon nanotubes,[35,36] C_{60} (ref. 36 and 37) and phenyl-C_{61}-butyric acid methyl ester (PCBM).[37] Up to date, C_{60} and PCBM are the only fullerene cages functionalized by pentafluorophenyl-quinolines. In this work, we demonstrate the chemical incorporation of a pentafluorophenyl-quinoline (FQ) derivative on the azafullerene $C_{59}N$ cage, towards

[a]*Theoretical and Physical Chemistry Institute, National Hellenic Research Foundation, 48 Vassileos Constantinou Avenue, 11635 Athens, Greece. E-mail: astergiou@eie.gr; tagmatar@eie.gr*

[b]*Department of Chemistry, University of Patras, University Campus, 26504 Rio-Patras, Greece*

† Electronic supplementary information (ESI) available: ^1H, ^{13}C and ^{19}F NMR, FT-IR spectra and ESI-MS for $C_{59}N$-FQ; FT-IR spectra of $C_{59}N$-FQH$^+$; Tauc plot of FQ, Job's, Hill and Stern–Volmer plots for $(H_2P)_2/C_{59}NFQH^+$; PL-spectra of $C_{59}N$-FQH$^+$; anodic and cathodic DPV graphs for $(H_2P)_2/C_{59}NFQ$ and $(H_2P)_2/C_{59}NFQH^+$; UV/Vis-PL cross-section spectra of $(H_2P)_2$. See DOI: 10.1039/d0ra06195f

a molecular recognition motif for the development of host–guest supramolecular assemblies featuring a hairpin-like face-to-face dimer porphyrin $(H_2P)_2$.

The quest for light harvesting antennas owing face-to-face porphyrins macrocycles was fueled by exploration of nature-mimicking molecular photosynthetic approaches.[38] P700, the electron donor unit of photosystem I, is considered to consist of two chlorophyll species (*a* and *a*′) axially coordinated by a histidine residual, resembling a face-to-face supramolecular porphyrin dimer.[39] Progress in artificial photosynthetic systems has met the expansion of fullerene chemistry, generating an interface where natural-inspired electron donors have been coupled to synthetic fullerene electron acceptors.[40,41] Porphyrin "tweezers" or "jaws" have attracted significant interest due to their versatile function as electron donor host-molecules and the simple, in general, chemistry required for their preparation.[42,43] Up to date, porphyrin tweezers have been efficiently employed as hosts for the molecular recognition of small electron withdrawing compounds[44] and fullerenes.[45–50]

The molecular recognition of acridine, with molecular structure resembling that of quinoline, due to strong electrostatic interactions by a metal-free porphyrin tweezer has been accomplished.[51,52] However, the recognition of pristine C_{60} fullerene by this type of metal-free $(H_2P)_2$ tweezers is weak,[46] requiring high excess of C_{60} in order to track detectable changes in the absorption features of the tweezer, especially of the Soret band arising from the $S_0 \rightarrow S_2$ optical transition of $(H_2P)_2$. Steric hindrance most likely restricts those species from efficiently approaching each other. Therefore, the quinoline heterocycle present within the **C_{59}N-FQ** dyad is, herein, exploited as flexible nanodomain capable of being sandwiched by the face-to-face porphyrin rings of the $(H_2P)_2$ tweezer. This, allows the development of effective electronic communication between $C_{59}N$ and $(H_2P)_2$ and mediated by **FQ** within the so-formed $(H_2P)_2$/**C_{59}N-FQ** assemblies. Moreover, we prepare the protonated form of **C_{59}N-FQ**, namely **C_{59}N-FQH$^+$**, benefited by the weak basic nature of the porphyrin heterocycles for empowering the development of electrostatic interactions between the individual species. Synergistic weak π–π interactions, electrostatic forces and weak hydrogen bonding between pentafluorophenyl-quinoline and the $(H_2P)_2$ macrocycle collectively stabilize the host–guest architecture. We perform complementary spectroscopic and electrochemical techniques to unveil and evaluate host–guest interactions in those nano-architectures. Specifically, electronic absorption, steady-state and time-resolved photoluminescence spectroscopy aided the assessment of the optical properties of $(H_2P)_2$/**C_{59}N-FQ** assemblies at the ground and excited states, while the redox properties were screened by electrochemistry.

Results and discussion

The pentafluorophenyl-quinoline derivative, 6-(4-hydroxylphenyl)-(2-perfluorophenyl)-4-phenyl-quinoline (**FQ**),[53] is chemically introduced on a pre-modified $C_{59}N$ cage bearing a –COOH unit.[5,8] For the covalent functionalization of the $C_{59}N$ cage with the quinoline derivative, the synthetic route shown in Scheme 1a is followed. Briefly, $(C_{59}N)_2$ is initially treated with di-(*tert*)butyl malonate diester at elevated temperature in the presence of oxygen, in order to proceed the nucleophilic attack of the malonate to the *in situ* generated $C_{59}N^+$ intermediate,[5] followed by thermally-induced decarboxylation to afford **C_{59}N-COOH**.[8] The latter compound is used for the incorporation of the 6-(4-hydroxylphenyl)-(2-perfluorophenyl)-4-phenyl-quinoline[53] *via* carbodiimide-mediated condensation yielding the **C_{59}N-FQ** dyad. ^{1}H, ^{13}C and ^{19}F NMR, and IR spectroscopy, together with ESI mass spectrometry, ascertained the structure of **C_{59}N-FQ**. In the ^{1}H NMR spectrum of **C_{59}N-FQ** (ESI, Fig. S1†) the characteristic signal at 5.07 ppm owed to the methylene protons next to the azafullerene cage, accompanied by the thirteen aromatic protons due to the **FQ** core in the region 7.3–8.3 ppm, is evident. In the ^{13}C NMR spectrum of **C_{59}N-FQ**, the typical signal at 168.2 ppm for the carbonyl ester is identified (ESI, Fig. S2†). Complementary, ^{19}F NMR assays reveal three distinct signals at −124, −153 and −161 ppm, due to the pentafluorophenyl ring within **FQ** (ESI, Fig. S3†). The formation of the ester bond in **C_{59}N-FQ** is further validated by ATR-IR spectroscopy, where the characteristic vibration of the ester carbonyl at 1758 cm^{-1}, accompanied by the absence of the band centred at 1711 cm^{-1} owed to the precursor carboxylic acid unit (ESI, Fig. S4†), is evolved. Ultimately, solid proof for the formation of **C_{59}N-FQ** is delivered by registering the corresponding $[M+1]^+$ ion at 1227.17 amu by ESI mass spectrometry (ESI, Fig. S5†). The high solubility of **C_{59}N-FQ** in common organic solvents, *i.e.* toluene, dichloromethane, chloroform and benzonitrile, enables not only performing a proper spectroscopic and electrochemical examination in liquid media, but also proceeding with the supramolecular integration of the porphyrin tweezer (Scheme 1b) yielding the $(H_2P)_2$/**C_{59}N-FQ** nanoarchitecture (Scheme 1c).

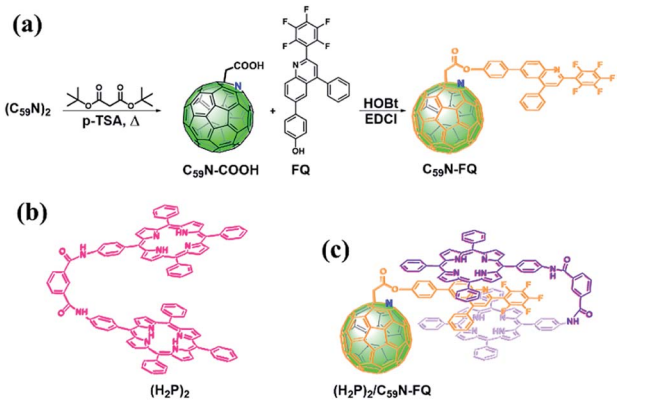

Scheme 1 (a) Synthetic procedure for the preparation of **C_{59}N-FQ**. (b) Structure of the co-facial dimer porphyrin tweezer $(H_2P)_2$. (c) Illustration of the supramolecular complex $(H_2P)_2$/**C_{59}N-FQ**.

In the UV-Vis electronic absorption spectrum of **C_{59}N-FQ** the main absorption features of $(C_{59}N)_2$ at 320, 440 and 600 nm, together with a new broad shoulder at 368 nm attributed to the attached **FQ** unit (Fig. 1a), are evident. Further, photoexcitation of **C_{59}N-FQ** at 320 and 340 nm, where **FQ** shows maximum absorbance, reveals quantitative quenching of the **FQ** emission

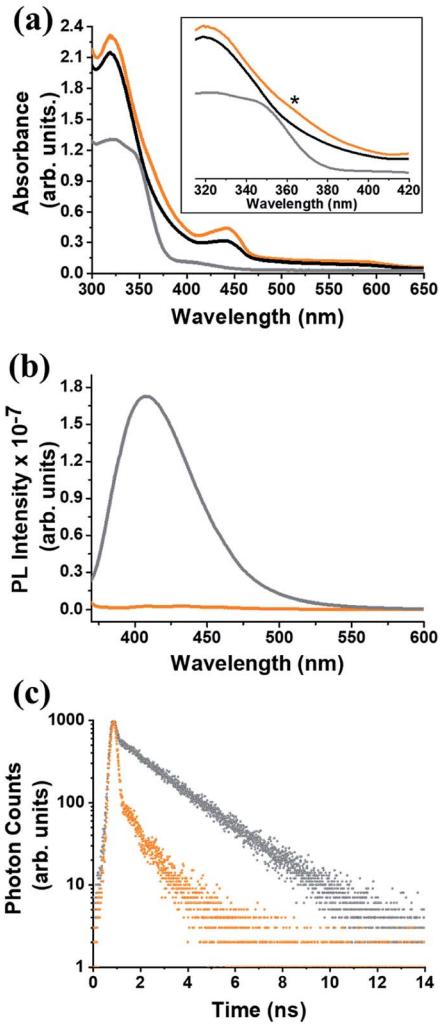

Fig. 1 (a) Electronic absorption UV-Vis spectra, (b) emission spectra at upon excitation at 340 nm, and (d) emission decay profiles (λ_{exc} 376 nm), for free **FQ** (gray), $(C_{59}N)_2$ (black) and C_{59}N-FQ (orange). All measurements were performed in toluene solutions. Inset: zoom of the 310–420 nm region, where a new absorption feature (marked with an asterisk) at 360 nm was observed for C_{59}N-FQ.

band centred at 401 nm (Fig. 1b), indicating strong electronic communication between the two species, C_{59}**N** and **FQ**, at the excited state. This is further supported by the examination of the emission decay profile of C_{59}**N-FQ** by the time-correlated-single-photon-counting (TCSPC) method, since a significantly shorter lifetime is recorded for the single excited state of the covalently attached **FQ** (~76 ps) in the C_{59}**N-FQ** dyad, as compared to the corresponding emission lifetime recorded for free **FQ** (1.9 ns), as shown in Fig. 1c. The fast deactivation of ^{1}FQ* suggests energy and/or electron transfer phenomena to occur in the presence of the azafullerene cage.

Insight into the redox properties of C_{59}**N-FQ** is given by complementary cyclic voltammetry (CV) assays. As presented in the summarized data of Table 1, the covalent attachment of **FQ** on C_{59}**N** anodically shifts the first oxidation potential E^1_{ox} by 0.41 V compared to that registered for free **FQ** (Fig. 2a), while cathodically shifts the first reduction potential E^1_{red} of

Table 1 Redox potentials and energy gaps (E_g) for **FQ**, $(C_{59}N)_2$ and C_{59}N-FQ

	Redox potentials (*vs.* Fc^+/Fc)				
Material	E^1_{ox}	E^1_{red}	E^2_{red}	E^3_{red}	E_g (eV)
FQ	+0.86	—	—	—	2.68[a]
$(C_{59}N)_2$	—	−1.20	−1.63	−2.20	1.40[b]
C_{59}N-FQ	+1.27	−1.36	−1.91	—	2.63[c]
(H_2P_2)	+0.38	−1.85	−2.14	—	2.23[d]

[a] Optical gap calculated from the Tauc plot, ESI, Fig. S6. [b] Optical gap value adopted from ref. 55. [c] Electrochemical gap based on Fig. 2a. [d] Electrochemical gap based on ESI, Fig. S10.

functionalized C_{59}**N** by 0.16 V compared to the value for $(C_{59}N)_2$. Based on the following equations (eqn (1) and (2)):[54]

$$\text{HOMO} = -(E_{ox} \textit{ vs. } Fc^+/Fc + 5.1)\ (\text{eV}) \quad (1)$$

$$\text{LUMO} = -(E_{red} \textit{ vs. } Fc^+/Fc + 5.1)\ (\text{eV}) \quad (2)$$

and the energy gap of **FQ** (ESI, Fig. S6†) and $(C_{59}N)_2$,[55] an energy level diagram is constructed (Fig. 2b). The energy alignment of the individual **FQ** and $(C_{59}N)_2$ suggests that the C_{59}**N-FQ** is an

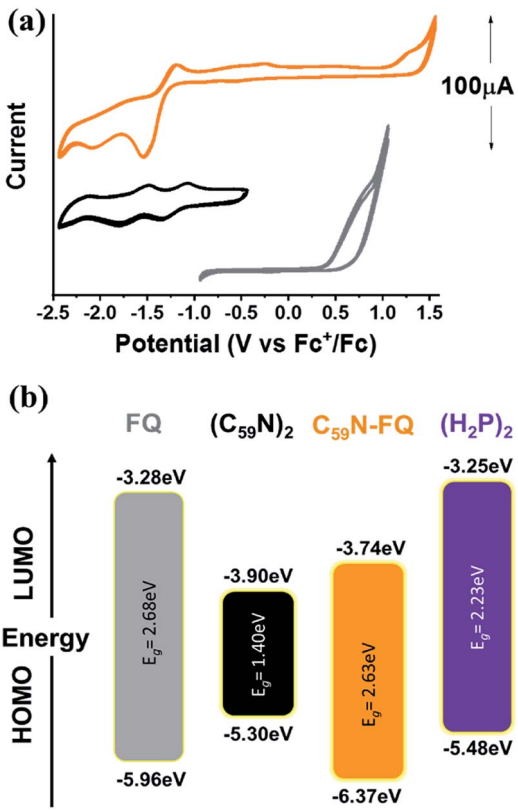

Fig. 2 (a) Cyclic voltammetry (CV) graphs for **FQ** (gray), $(C_{59}N)_2$ (black) and C_{59}N-FQ (orange) *vs.* Fc^+/Fc. CV curves recorded in N_2 saturated toluene : acetonitrile (vol/vol 1 : 4) with 0.1 M $TBAPF_6$ as electrolyte and 50 mV s^{-1} scan rate. (b) Energy level diagram constructed from the data presented in Table 1.

electron donor–acceptor dyad, where **FQ** is the donor and **C_{59}N** the acceptor. Accordingly, we may calculate the HOMO–LUMO energy levels of the **C_{59}N-FQ** dyad by the observed E^1_{ox} and E^1_{red} values, as −6.37 and −3.81 eV, respectively. Taking into consideration the HOMO–LUMO energy levels of the **$(H_2P)_2$** tweezer, the energy alignment of the supramolecular **$(H_2P)_2$/C_{59}N-FQ** host–guest assemblies was favorable towards a p–n junction, where the **$(H_2P)_2$** tweezer is the electron donor and the **C_{59}N-FQ** is the electron acceptor. In previous studies, analogous covalent dyads consisting of **FQ** and the C_{60} fullerene have been successfully integrated in organic solar cells as electron acceptors utilizing poly-(3-hexyl thiophene) (P3HT), a widely adopted electron donor polymer with similar to **$(H_2P)_2$** tweezer HOMO–LUMO energy levels, as electron donor.[36]

We firstly explore the complexation dynamics between **C_{59}N-FQ** and **$(H_2P)_2$** tweezer by UV-Vis electronic absorption, steady-state and time-resolved fluorescence emission spectroscopy. As depicted in Fig. 3a–d, upon incremental addition of **C_{59}N-FQ** (0–2 equivalents) in a benzonitrile solution of **$(H_2P)_2$**, negligible changes are recorded in the UV-Vis spectra of **$(H_2P)_2$**, namely a 2% decrement of the absorption intensity of the Soret band at 420 nm and a 4% quenching of the emission intensity of **$(H_2P)_2$** under excitation of the Soret band. Evidently, a weak interaction between the individual species occurs, which is also verified by the analysis of the time-resolved fluorescence spectra of **$(H_2P)_2$** in the presence of 2 equivalents of **C_{59}N-FQ**, where the decay trace is best fitted by a mono-exponential model giving a fluorescence lifetime of 10 ns, corresponding to that of non-complexed **$(H_2P)_2$**.

Taking advantage of the low basicity of the quinoline domain, we next treat **C_{59}N-FQ** with an excess of trifluoroacetic acid leading to the corresponding protonated **C_{59}N-FQH$^+$** species. The protonation of **C_{59}N-FQ** is monitored by FT-IR spectroscopy (ESI, Fig. S7†) and discrete spectra profiles are obtained, while the process is fully reversible upon addition of excess triethylamine. More specific, it is known that protonation of the quinoline nitrogen atom results to a shielding effect to the neighboring phenyl groups where the oxygen atom resides, as it was previously demonstrated by ^{1}H NMR assays.[53] The latter effect strongly affects the C=O stretching vibration of the ester group connecting the **C_{59}N** cage and the quinoline derivative. As a result, the C=O stretching mode registered at 1758 cm^{-1} for **C_{59}N-FQ** is shifted by 24 cm^{-1} for protonated **C_{59}N-FQH$^+$** at 1734 cm^{-1}.

Focusing on the impact of the protonated quinoline in the supramolecular complexation of **C_{59}N-FQH$^+$** with the **$(H_2P)_2$** tweezer, a series of titration assays are performed. Please note that NMR titration assays are hampered due to overlap of the signals of interest, namely the host molecules **C_{59}N-FQ** and **C_{59}N-FQH$^+$**, contribute ^{1}H-signals arising due to the **FQ** domain which overlap with the pyrrolic ^{1}H of the porphyrin dimer **$(H_2P)_2$** tweezer. In addition, ^{19}F NMR and especially FAXS (fluorine chemical shift anisotropy and exchange for screening) and *n*-FABS (*n*-fluorine atoms for biochemical screening), methods developed for competitive binding assays in biosystems, require fluorinated fragments with strong sharp singlet signals, in contrast to the C–F groups of the pentafluorophenyl moiety which are strongly coupled resulting to complex splitting patterns as shown in Fig. S3.† Nevertheless, the electronic absorption spectrum of **$(H_2P)_2$** upon incremental additions of **C_{59}N-FQH$^+$** (up to 2 equivalents) reveal enhanced interactions as expressed by the suppression of the Soret band absorption by 15%, accompanied by 18% quenching to the fluorescence emission intensity of the **$(H_2P)_2$** tweezer (Fig. 3e–g). Further, time-resolved fluorescence emission spectroscopy reveals the evolution of a new short-lived component (10% population, τ = 1 ns), which is attributed to the deactivation pathway of the photoexcited electron from the singlet excited state of **$(H_2P)_2$** to **C_{59}N-FQH$^+$** (Fig. 3h). These findings underscore the impact of the positively charged guests, in the form of

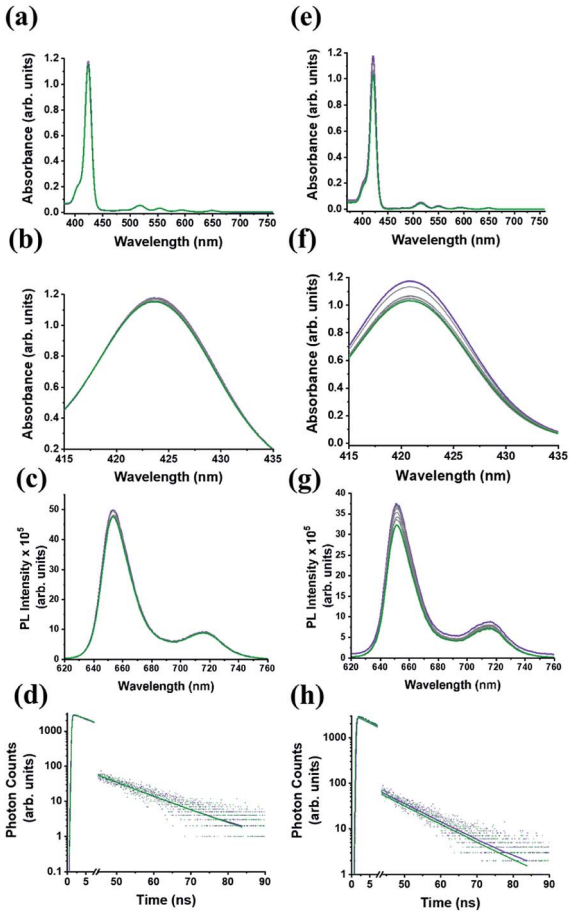

Fig. 3 (a and e) UV-Vis electronic absorption spectra of $(H_2P)_2$ tweezer (purple) upon incremental additions of up to 2 equivalents (olive) of C_{59}N-FQ and C_{59}N-FQH$^+$, respectively. (b and f) Zoom of the corresponding Soret band regions. In all spectra the absorbance of C_{59}N-FQ and C_{59}N-FQH$^+$ is subtracted. (c and g) Steady-state fluorescence emission spectra of $(H_2P)_2$ tweezer (purple) upon excitation of the Soret band (λ_{exc} 420 nm) upon incremental additions of up to 2 equivalents (olive) of C_{59}N-FQ and C_{59}N-FQH$^+$, respectively. (d and h) Emission decay profiles (λ_{exc} 440 nm, probed at 650 nm) of $(H_2P)_2$ tweezer (purple) upon incremental additions of up to 2 equivalents (olive) of C_{59}N-FQ and C_{59}N-FQH$^+$, respectively. Dotted lines represent the decay trace, while solid lines represent the mathematical fitting of the decay spectra. All spectra were recorded in benzonitrile at 1×10^{-6} M concentration of the $(H_2P)_2$ tweezer.

protonated FQH$^+$ domains, to the hosting ability of the co-facial metal-free porphyrin dimer and are fully in line with previously reported assemblies centered on acridinium cations.[51,52]

For the **$(H_2P)_2$/C_{59}N-FQ** system, both the UV-Vis and PL emission changes during the titration assays were negligible suggesting the absence of notable interactions. In contrast, the changes observed in the UV-Vis and PL spectra for the **$(H_2P)_2$/C_{59}N-FQH$^+$** system allowed us to obtain a rough estimation for the stoichiometry and the binding constant. In order to further validate the presence of complexation events between the **C_{59}N-FQH$^+$** and the tweezer, we constructed the corresponding Job plot (ESI, Fig. S8a†) for unravelling the stoichiometry as well as the Hill plot (ESI, Fig. S8b†) to evaluate the binding constants. Specifically, the Job's plot for the **$(H_2P)_2$/C_{59}N-FQH$^+$** system suggests the co-existence 1 : 1 and 1 : 2 stoichiometries,[56] while from the Hill plot the binding constant was calculated to be 3.17 $\times$ 10^2 M. Moreover, from the Stern–Volmer plot derived from the fluorescence titration we find a K_{SV} value of 2.6 $\times$ 10^4 M^{-1} (ESI, Fig. S8c†) and by taking into account the new short-lived component revealed form time-resolved fluorescence emission spectroscopy, a dynamic quenching mechanism is proposed. An estimation of the charge separation dynamics can be deduced by eqn (3) and (4):

$$k_{CS} = (1/\tau)_{(H_2P)_2/C_2N\text{-}FQH^+} - (1/\tau)_{(H_2P)_2} \quad (3)$$

$$\Phi_{CS} = k_{CS}/(1/\tau)_{(H_2P)_2/C_2N\text{-}FQH^+} \quad (4)$$

where τ is the fluorescence lifetime of the free **$(H_2P)_2$** in solution or the **$(H_2P)_2$** host within the supramolecular **$(H_2P)_2$/C_{59}N-FQH$^+$** host–guest assembly, allowing us to calculate the charge separation rate constant (k_{CS}) and the charge separation quantum yield (Φ_{CS}) for the **$(H_2P)_2$/C_{59}N-FQH$^+$** host–guest assembly, based on the fluorescence decay values recorded by TCSPC spectroscopy. The k_{CS} and Φ_{CS} values are found as high as 0.9 $\times$ 10^9 s^{-1} and 0.9, respectively, suggesting a slow charge separation with high quantum yield.

A comprehensive examination of the UV-Vis spectrum of **C_{59}N-FQH$^+$** reveals a slight broadening of the absorption spectra in the range of 300–380 nm, where both the azafullerene cage and the chemically attached protonated quinoline derivative absorb light. This feature is further accompanied by a weak band centred at 420 nm, as compared to the absorption profile of neutral **C_{59}N-FQ** (Fig. 4a). In addition, the protonation of quinoline induces a more intense variation to the fluorescence emission profile of **C_{59}N-FQH$^+$**. It is known that quinoline derivatives are sensitive to charge delocalization and specifically to protonation of the nitrogen atom.[57] Hence, the protonated quinoline domain impacts the emission spectrum of **C_{59}N-FQH$^+$**, since upon photoexcitation of the quinoline core (λ_{exc} 340 nm), a red-shifted and quenched emission band centered at 440 nm is observed (Fig. 4b). Moreover, an excitation-dependent emission spectrum is registered for **C_{59}N-FQH$^+$** (ESI, Fig. S9†), in contrast to that derived from neutral **C_{59}N-FQ**. As long as the emission spectra of **C_{59}N-FQH$^+$** are found independent of the concentration, the presence of excimers is excluded.[58] In general, protonation of quinolines lowers the energy of their

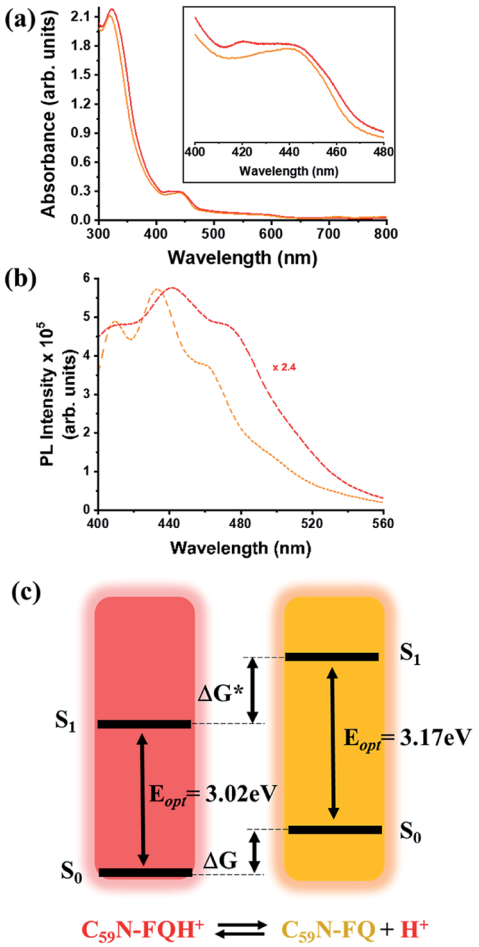

Fig. 4 (a) UV-Vis and (b) fluorescence emission spectra (λ_{exc} 340 nm) of C_{59}N-FQ (orange) and C_{59}N-FQH$^+$ (red), acquired in benzonitrile. (c) Schematic illustration of the Förster cycle.

singlet excited state and the absorption band drifts to lower energy.[57] Therefore we assume that the properties of **C_{59}N-FQH$^+$** are related to the photo-basicity of quinolines as described by the Förster cycle (Fig. 4c). Neutral quinolines show increased pK_a values during photoexcitation (p$K_a^* >$ pK_a) inducing proton capture at the singlet excited states.[59] Considering that the complexation assays of **C_{59}N-FQH$^+$** for hosting the **$(H_2P)_2$** tweezer are performed in aprotic benzonitrile (*cf.* Fig. 3), dissociation to the neutral state by proton release to the solvent medium is blocked and therefore **C_{59}N-FQH$^+$** remains charged under photoexcitation. Evidently, the tetrapyrrole core of the **$(H_2P)_2$** tweezer, which is a weak base, favors the interactions with positively charged species, thus allowing electronic communication within the supramolecular assembly **$(H_2P)_2$/C_{59}N-FQH$^+$** both at the ground and the excited state. It should be mentioned that protonation of metal-free **$(H_2P)_2$** is not observed, since the corresponding absorption spectrum remains unaltered.

Finally, we explore the electronic communication between the **$(H_2P)_2$** tweezer and the **C_{59}N-FQ** derivatives into an electrochemical environment *via* differential pulse voltammetry

(DPV) studies. DPV is selected as a sensitive electrochemical technique capable to the feasibility of the redox processes arose from the supramolecular assembly. Therefore, we monitor the redox features of $(H_2P)_2$ upon incremental additions of up to 2 equivalents of C_{59}N-FQ and C_{59}N-FQH$^+$, respectively, as compared to the corresponding features of the individual $(H_2P)_2$, C_{59}N-FQ and C_{59}N-FQH$^+$ species in nitrogen saturated solutions of 0.1 M $TBAPF_6$ in benzonitrile. Firstly, we perform anodic and cathodic scans to address the redox potential of the individuals and evaluate the reversibility of the redox processes, while also to monitor the potent impact of the azafullerene derivatives to the oxidation and reduction properties of the $(H_2P)_2$ tweezer (ESI, Fig. S10†). The recorded DPV curves display strong interactions at working electrode interface between the host–guest species. Then, we focus at the HOMO level of the tweezer and the LUMO level of the quinoline-modified C_{59}N cage at the neutral and charged state of the quinoline domain, namely we monitor the anodic wave of $(H_2P)_2$ tweezer oxidation and the cathodic wave of the first reduction of the azafullerene cage within C_{59}N-FQ and C_{59}N-FQH$^+$. Prior each titration step, the system is allowed to reach equilibrium in nitrogen saturated benzonitrile solutions with 0.1 M $TBAPF_6$ as the supporting electrolyte. These redox studies are presented in Fig. 5a and b. Analysis of the registered oxidation potentials for the $(H_2P)_2$ tweezer and the reduction potential of the pentafluoroquinoline-functionalized azafullerene cages show a slightly different redox response of $(H_2P)_2$/C_{59}N-FQ and $(H_2P)_2$/C_{59}N-FQH$^+$ (Fig. 5c). Evidently, for the $(H_2P)_2$/C_{59}N-FQ host–guest assemblies the oxidation potential of $(H_2P)_2$ tweezer and the first reduction potential of the azafullerene cage within C_{59}N-FQ, remain almost unaltered during the different host–guest ratios. In contrast, the $(H_2P)_2$/C_{59}N-FQH$^+$ host–guest assemblies display more intense changes. More specific, in the presence of ~1.5 eq. of C_{59}N-FQH$^+$ guest, the oxidation potential of $(H_2P)_2$ host display a cathodic shift by 132 mV, suggesting easier oxidation, accompanied by the anodic shift of the first reduction potential of the guest by 83 mV, indicating easier reduction. These observations are further probed by means of charge separation efficiency. The Gibbs energy of photoinduced electron transfer ($\Delta_{ET}G^0$) between the $(H_2P)_2$ host (electron donor) and the C_{59}N-FQ or C_{59}N-FQH$^+$ guest (electron acceptor) can be approximated by eqn (5):[60]

$$\Delta_{ET}G^{o} = N_A\left[e\left[E^{o}_{(D^{+\cdot}/D)} - E^{o}_{(A/A^{-\cdot})}\right] + w_{(D^{+\cdot}A^{-\cdot})} - w_{(DA)}\right] - \Delta E_{0,0} \quad (5)$$

where e is the elementary charge, N_A is the Avogadro constant, $E^{o}_{(D^{+\cdot}/D)}$ is the electrode potential of the donor radical cation resulting from the electron transfer, $E^{o}_{(A/A^{-\cdot})}$ the electrode potential of the acceptor radical anion, while the $\Delta E_{0,0}$ is the energy level of the singlet excited state of the electron donor (ESI, Fig. S11†). The $w(D^{+\cdot}A^{-\cdot})$ and $w_{(DA)}$ are electrostatic work terms accounting for the effect of Coulombic interactions. Eqn (5) is usually referred as the "Rehm–Weller relation". The Gibbs energy for the ion pair separation (ΔG_{CS}) in benzonitrile is represented by eqn (6), based on the Gibbs energy of charge recombination (ΔG_{CR}, eqn (7)) and the static energy (ΔG_s, eqn (8)):[61,62]

$$-\Delta G_{CS} = \Delta E_{0,0} - (-\Delta G_{CR}) \quad (6)$$

$$-\Delta G_{CR} = e\left[E^{o}_{(D^{+\cdot}/D)} - E^{o}_{(A/A^{-\cdot})}\right] + \Delta G_S \quad (7)$$

$$\Delta G_s = e^2/4\pi\varepsilon_0[(1/R_{host} + 1/R_{guest} - 1/R_{host-guest})(1/\varepsilon_S) - (1/R_{host} + 1/R_{guest})(1/\varepsilon_S)] \quad (8)$$

where ε_0 is the vacuum permittivity, ε_S is the dielectric constant of the solvent used for the photophysical studies, ε_R is the dielectric constant of the solvent used for the determination of redox potential, R_{guest} is the radius of the guest molecule, R_{host} is the radius of the host molecule and $R_{host-guest}$ is center-to-center distance between the host and guest components in the supramolecular assembly.[39]

Based on eqn (6)–(8) we can estimate the variation of the ΔG_{CS} value in respect to the host : guest ratio. As presented in Fig. 5d, for both $(H_2P)_2$/C_{59}N-FQ and $(H_2P)_2$/C_{59}N-FQH$^+$ assemblies, the Gibbs energy of charge separation is negative, manifesting an exothermic process and thus a thermodynamically favored mechanism. Moreover, for the $(H_2P)_2$/C_{59}N-FQH$^+$ assembly we observe a sharp contrast in the region of 1.0–1.5 eq. of C_{59}N-FQH$^+$. These values correspond to a molar fraction of $(H_2P)_2$: C_{59}N-FQH$^+$ ranging between 1 : 1 to 1 : 1.5 (X_{guest} = 0.5–

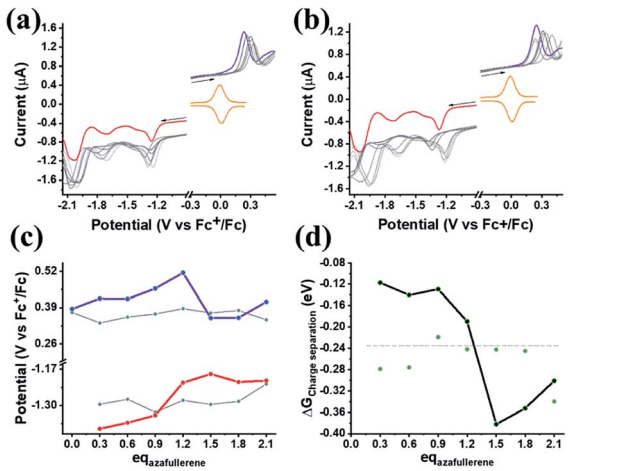

Fig. 5 (a and b) DPV curves recorded upon incremental additions of up to 2.1 equivalents (gray lines) of C_{59}N-FQ and C_{59}N-FQH$^+$, respectively. Purple line represents the DPV oxidation wave of free $(H_2P)_2$, red line refers to the reduction wave of the azafullerene cage within C_{59}N-FQ and C_{59}N-FQH$^+$, while orange line displays the Fc$^+$/Fc redox pair employed as internal reference. All graphs recorded in N_2-saturated solutions of 0.3 mM $(H_2P)_2$ in benzonitrile with 0.1 M $TBAPF_6$ as the supporting electrolyte at room temperature with scan rate 0.01 V s^{-1}. (c) Plots for the $(H_2P)_2$ oxidation potential (purple) and the first reduction potential for the azafullerene cage of C_{59}N-FQH$^+$ (red) *versus* the different host : guest ratios. The gray lines represent the corresponding plots in the presence of the C_{59}N-FQ derivative. (d) Plots for the Gibbs energy of charge separation (ΔG_{CS}) *versus* the host–guest ratio for the $(H_2P)_2$/C_{59}N-FQ (gray) and $(H_2P)_2$/C_{59}N-FQH$^+$ (black) assemblies. The dotted line represents the level of the ΔG_{CS} calculated *via* the redox potentials of the non-interacting individuals.

0.6) for the used solutions of 0.3 mM in benzonitrile, matching the stoichiometry calculated from the Job's plot for 1×10^{-6} M solutions in benzonitrile (ESI, Fig. S8a†). A maximum $-\Delta G_{CS}$ of $\sim$−0.4 eV is registered in the presence of 1.5 eq. of **C_{59}N-FQH$^+$** indicating that the formation of the host–guest complexes requires a slight excess of the guest molecules in order to be activated. Concluding, the redox behavior of the **$(H_2P)_2$/C_{59}N-FQ** and **$(H_2P)_2$/C_{59}N-FQH$^+$** mixtures complement the corresponding photophysical profiles, suggesting that the protonation of the quinoline domain induces enhanced interactions between the individuals and enables the formation of relatively stable host–guest complexes enabling the electronic communication of the porphyrin tweezer and the azafullerene cage.

Experimental

General

All reagents were used as received. The solvents were dried using standard techniques. Reactions were monitored by thin layer chromatography on silica gel 60 F_{254} aluminum plates. Products were isolated by column chromatography (silica gel 60, particle size 0.004–0.063 mm). **FQ**,[53] porphyrin-dimer **$(H_2P)_2$** tweezer[45] and **C_{59}N-COOH**[5,8] were synthesized according to published procedures.

Instrumentation

^{1}H, ^{13}C and ^{19}F Nuclear Magnetic Resonance (NMR) spectra were recorded on a Bruker Avance (Bruker BioSpin GmbH, Magnet Division, Karlsruhe, Germany) DPX 600 13, 150 92 and 564 63 MHz spectrometer, respectively, in deuterated solvents containing TMS as internal standard. The chemical shifts are given in ppm relative to the appropriate solvent peak at standard reference. The resonance multiplicity is indicated as s (singlet), d (doublet), t (triplet), dd (doublet of doublets), td (triplet of doublets) and m (multiplet). Electrospray Ionization Mass Spectroscopy (ESI-MS) measurements were performed using an amaZon SL ion trap of Bruker Daltonics GmbH, Bremen Germany. UV-Vis spectra were recorded on a Perkin Elmer Lambda 19 spectrometer. Fluorescence spectra were recorded in toluene solutions on a Fluorolog-3 Jobin Yvon-Spex spectrofluorometer (model GL3-21) equipped with a UV-Vis detector (200–800 nm) operated at room temperature. TCSPC spectra recorded *via* the Horiba Fluorohub single photon counting controller. IR spectra were recorded on Bruker Equinox 55 FTIR spectrometer equipped with a Pike Miracle Ge ATR accessory. Electrochemistry studies were performed by using a standard three-electrode cell. Glassy carbon was used as a working electrode and platinum wire and platinum mesh were used as pseudo-reference and counter electrodes, respectively. A mixture of toluene/acetonitrile (4 : 1) was used as the solvent and ferrocene was employed as an internal reference for the CV studies. DPV studies were performed in benzonitrile. $TBAPF_6$ (98%) was recrystallized three times from acetone and dried under vacuum at 100 °C before used as an electrolyte with 0.1 M concentration for the CV and DPV studies. Before each experiment, the cell was purged with high purity N_2 for 15 min and the inert gas was turned to "blanket mode". The working electrode was cleaned before each experiment (also in between the titration steps in DPV studies) through polishing with a cloth and 6, 3 and 1 mm diamond pastes. CV measurements were recorded by using an EG&G Princeton Applied Research potentiostat/galvanostat model VersaSTAT 4 instrument connected to a personal computer running the VersaStudio software. DPV measurements were recorded by AUTOLAB PGSTAT128N potentiostat/galvanostat instrument connected to a personal computer running the Nova 2.1 software.

Synthetic procedures

Synthesis of C_{59}N-FQ. **C_{59}N-COOH** (59 mg, 0.075 mmol) was mixed with **FQ** (104 mg, 0.225 mmol) in 100 mL dry $CHCl_3$. Then, HOBt (33 mg, 0.247 mmol) and EDC·HCl (47 mg, 0.247 mmol) were also added and the mixture was stirred for 8 h. The reaction was monitored by TLC (SiO_2) with $CHCl_3$ as eluent and two greenish fullerene spots were evident. The solvent was removed by rotary evaporation and the residue was dissolved in CS_2 and purified by column chromatography (SiO_2) with toluene as eluent. Only one greenish fraction was eluted, evaporated to 2–3 mL and the product precipitated by addition of cold hexane. The solid collected by centrifugation (300 rpm for 5 min) and dried under vacuum. ^{1}H NMR ($CDCl_3$): 8.32 (1H, d, $J = 4.35$ Hz), 8.19 (1H, d, $J = 0.2$ Hz), 8.07 (1H, dd, $J_1 = 0.84$ Hz, $J_2 = 0.87$ Hz), 7.74 (2H, d, $J = 4.29$ Hz), 7.61–7.51 (8H, m) and 5.1 (2H, s) ppm. ^{13}C NMR ($CDCl_3$): 168.21 (C═O), 155.23, 150.48, 149.76, 147.92, 147.67, 147.53, 147.42, 147.07, 146.77, 146.71, 146.43, 146.04, 146.27, 144.59, 144.53, 144.15, 143.30, 142.98, 142.29, 141.95, 141.60, 141.27, 141.24, 141.14, 139.89, 137.74, 137.31, 134.48, 130.85, 129.72, 129.58, 128.94, 128.91, 126.37, 124.50, 123.75, 123.47, 122.30 and 76.98 ppm. ^{19}F NMR ($CDCl_3$): −161 (2H, td, $J_1 = 4.17$ Hz, $J_2 = 3.66$ Hz, $J_3 = 4.35$ Hz), −153 (1H, t, $J = 11.04$ Hz) and −142 (2H, dd, $J_1 = 4.17$ Hz, $J_2 = 4.26$ Hz) ppm. ESI-MS: calculated m/z for $C_{88}H_{15}F_5N_2O_2$ [M + 1]: 1227.11; found: 1227.17.

Synthesis of C_{59}N-FQH$^+$. 10 mg of **C_{59}N-FQ** were dissolved in 10 mL chloroform at room temperature and the was immersed into an ice-bath, followed by the dropwise addition of excess glacial acetic acid ($\sim$1 mL) under stirring. The mixture was allowed to reach room temperature under stirring and then evaporated to dryness under vacuum. The solid residue was dissolved in a minimum amount of chloroform, cooled in the fridge and precipitated by addition of cold hexane. **C_{59}N-FQH$^+$** was recovered by centrifugation, dried under vacuum and collected as brown powder (8 mg).

Conclusions

A new azafullerene **(C_{59}N)** derivative covalently carrying a pentafluoroquinoline (**FQ**) was synthesized and fully characterized. The evidenced strong intramolecular electronic communication between the pentafluoroquinoline and azafullerene cage allowed us to exploit the quinoline domain as guest for hosting the **$(H_2P)_2$** porphyrin tweezer. Interestingly, protonation of the quinoline heterocycle enables even stronger interactions, due to

enhanced electrostatic attraction forces occurring between the $(H_2P)_2$ host and the protonated $C_{59}N$-FQH$^+$ guest species within the $(H_2P)_2/C_{59}N$-FQH$^+$ supramolecular nanoassembly. Photophysical studies revealed detectable host–guest interactions in $(H_2P)_2/C_{59}N$-FQH$^+$ represented by the slight decrement of the Soret band intensity of $(H_2P)_2$, complemented by partial quenching of the fluorescence emission of $(H_2P)_2$, in contrast to the corresponding $(H_2P)_2/C_{59}N$-FQ where almost negligible differences were observed. Analysis of the time-resolved fluorescence spectra uncovered a new decay component of 1 ns for $(H_2P)_2/C_{59}N$-FQH$^+$, attributed to the deactivation of the singlet excited state of $(H_2P)_2$ to the azafullerene. In addition, differential pulse voltammetry titration assays displayed intense changes for the oxidation potential of $(H_2P)_2$ and the first reduction potential of the azafullerene cage within $C_{59}N$-FQH$^+$, suggesting easier oxidation of the host and easier reduction of the guest, respectively, in the range of 1.0–1.5 eq. of guest. Overall, the beneficial effect of the protonated quinoline domain in the formation of the host–guest supramolecular complexes was further confirmed by the calculated value of Gibbs free energy for charge separation ΔG_{CS}. Here, it is the maximum value of around −0.4 eV registered for the $(H_2P)_2/C_{59}N$-FQH$^+$ assembly, which guarantees as an energetic favorable process the electronic communication between $(H_2P)_2$ and $C_{59}N$. Collectively, we presented a very first investigation concerning the electronic interactions of $C_{59}N$ with molecular porphyrin-dimer $(H_2P)_2$ tweezers *via* a host–guest approach mediated by a versatile amphoteric heterocycle motif of a pentafluoroquinoline derivative conjugated on the azafullerene cage.

Conflicts of interest

There are no conflicts to declare.

Acknowledgements

Partial financial support of this work by the project "Advanced Materials and Devices" (MIS 5002409), which is implemented under the "Action for the Strategic Development on the Research and Technological Sector", funded by the Operational Program "Competitiveness, Entrepreneurship and Innovation" (NSRF 2014–2020) and co-financed by Greece and the European Union (European Regional Development Fund) is acknowledged.

Notes and references

1 J. C. Hummelen, M. Prato and F. Wudl, There Is a Hole in My Bucky, *J. Am. Chem. Soc.*, 1995, **117**, 7003–7004.
2 J. C. Hummelen, B. Knight, J. Pavlovich, R. González and F. Wudl, Isolation of the Heterofullerene $C_{59}N$ as Its Dimer $(C_{59}N)_2$, *Science*, 1995, **269**, 1554.
3 O. Vostrowsky and A. Hirsch, Heterofullerenes, *Chem. Rev.*, 2006, **106**, 5191–5207.
4 G. Rotas and N. Tagmatarchis, Azafullerene $C_{59}N$ in Donor–Acceptor Dyads: Synthetic Approaches and Properties, *Chem.–Eur. J.*, 2016, **22**, 1206–1214.
5 F. Hauke and A. Hirsch, $C_{59}N^+$: a key intermediate in azaheterofullerene chemistry, *Tetrahedron*, 2001, **57**, 3697–3708.
6 F. Hauke, S. Atalick, D. M. Guldi, J. Mack, L. T. Scott and A. Hirsch, Molecular satellite dishes: attaching parabolic and planar arenes to heterofullerenes, *Chem. Commun.*, 2004, 766–767.
7 F. Hauke, A. Hirsch, S.-G. Liu, L. Echegoyen, A. Swartz, C. Luo and D. M. Guldi, Evidence of Pronounced Electronic Coupling in a Directly Bonded Fullerene–Ferrocene Dyad, *ChemPhysChem*, 2002, **3**, 195–205.
8 G. Rotas, J. Ranta, A. Efimov, M. Niemi, H. Lemmetyinen, N. Tkachenko and N. Tagmatarchis, Azafullerene $C_{59}N$–Phthalocyanine Dyad: Synthesis, Characterisation and Photoinduced Electron Transfer, *ChemPhysChem*, 2012, **13**, 1246–1254.
9 G. Rotas, G. Charalambidis, L. Glätzl, D. T. Gryko, A. Kahnt, A. G. Coutsolelos and N. Tagmatarchis, A corrole–azafullerene dyad: synthesis, characterization, electronic interactions and photoinduced charge separation, *Chem. Commun.*, 2013, **49**, 9128–9130.
10 L. Martín-Gomis, G. Rotas, K. Ohkubo, F. Fernández-Lázaro, S. Fukuzumi, N. Tagmatarchis and Á. Sastre-Santos, Does a nitrogen matter? Synthesis and photoinduced electron transfer of perylenediimide donors covalently linked to $C_{59}N$ and C60 acceptors, *Nanoscale*, 2015, **7**, 7437–7444.
11 G. Rotas, K. Stranius, N. Tkachenko and N. Tagmatarchis, Ultralong 20 Milliseconds Charge Separation Lifetime for Photoilluminated Oligophenylenevinylene–Azafullerene Systems, *Adv. Funct. Mater.*, 2018, **28**, 1702278.
12 U. Reuther and A. Hirsch, Pyrrole-embedded [60]fullerenes, *Chem. Commun.*, 1998, 1401–1402.
13 N. B. Shustova, I. V. Kuvychko, A. A. Popov, M. von Delius, L. Dunsch, O. P. Anderson, A. Hirsch, S. H. Strauss and O. V. Boltalina, Nitrogen Directs Multiple Radical Additions to the 9,9′-Bi-1-aza(C60-Ih)[5,6]fullerene: X-ray Structure of 6,9,12,15,18-$C_{59}N$(CF3)5, *Angew. Chem., Int. Ed.*, 2011, **50**, 5537–5540.
14 K. Y. Amsharov, J. Holzwarth, K. Roshchyna, D. I. Sharapa, F. Hampel and A. Hirsch, Synthesis, Structural Characterization, and Crystal Packing of the Elusive Pentachlorinated Azafullerene C59NCl5, *Chem.–Eur. J.*, 2017, **23**, 9014–9017.
15 R. Neubauer, F. W. Heinemann, F. Hampel, Y. Rubin and A. Hirsch, Pentaarylazafullerenes and their Triaryldihydro and Tetraarylmonohydro Precursors, *Angew. Chem., Int. Ed.*, 2012, **51**, 11722–11726.
16 R. Eigler, F. W. Heinemann and A. Hirsch, Hydro-aza-(C59N) fullerenes: Formation Mechanism and Hydrogen Substitution, *Chem.–Eur. J.*, 2016, **22**, 13575–13581.
17 F. Hauke and A. Hirsch, Regioselective formation of highly functionalised heterofullerenes: pentamalonates of RCN involving an octahedral addition pattern, *Chem. Commun.*, 2001, 1316–1317.

18 A. Stergiou, K. Asad, A. Kourtellaris, N. Chronakis and N. Tagmatarchis, Tether-Directed Regioselective Synthesis of an Equatorialface Bisadduct of Azafullerene Using Cyclo-[2]-octylmalonate, *Chem.–Eur. J.*, 2019, **25**, 5751–5756.

19 S. E. Lewis, Cycloparaphenylenes and related nanohoops, *Chem. Soc. Rev.*, 2015, **44**, 2221–2304.

20 Y. Segawa, A. Yagi, K. Matsui and K. Itami, Design and Synthesis of Carbon Nanotube Segments, *Angew. Chem., Int. Ed.*, 2016, **55**, 5136–5158.

21 D. Wu, W. Cheng, X. Ban and J. Xia, Cycloparaphenylenes (CPPs): An Overview of Synthesis, Properties, and Potential Applications, *Asian J. Org. Chem.*, 2018, **7**, 2161–2181.

22 Y. Xu and M. von Delius, The Supramolecular Chemistry of Strained Carbon Nanohoops, *Angew. Chem., Int. Ed.*, 2020, **59**, 559–573.

23 Y. Xu, B. Wang, R. Kaur, M. B. Minameyer, M. Bothe, T. Drewello, D. M. Guldi and M. von Delius, A Supramolecular [10]CPP Junction Enables Efficient Electron Transfer in Modular Porphyrin–[10]CPP⊃Fullerene Complexes, *Angew. Chem., Int. Ed.*, 2018, **57**, 11549–11553.

24 J. Rio, S. Beeck, G. Rotas, S. Ahles, D. Jacquemin, N. Tagmatarchis, C. Ewels and H. A. Wegner, Electronic Communication between two [10]cycloparaphenylenes and Bis(azafullerene) (C59N)2 Induced by Cooperative Complexation, *Angew. Chem., Int. Ed.*, 2018, **57**, 6930–6934.

25 A. Stergiou, J. Rio, J. H. Griwatz, D. Arčon, H. A. Wegner, C. P. Ewels and N. Tagmatarchis, A Long-Lived Azafullerenyl Radical Stabilized by Supramolecular Shielding with a [10]Cycloparaphenylene, *Angew. Chem., Int. Ed.*, 2019, **58**, 17745–17750.

26 G. Rotas, L. Martín-Gomis, K. Ohkubo, F. Fernández-Lázaro, S. Fukuzumi, N. Tagmatarchis and Á. Sastre-Santos, Axially Substituted Silicon Phthalocyanine as Electron Donor in a Dyad and Triad with Azafullerene as Electron Acceptor for Photoinduced Charge Separation, *Chem.–Eur. J.*, 2016, **22**, 15137–15143.

27 F. Hauke, S. Atalick, D. M. Guldi and A. Hirsch, Covalently linked heterofullerene–porphyrin conjugates; new model systems for long-lived intramolecular charge separation, *Tetrahedron*, 2006, **62**, 1923–1927.

28 F. Hauke, A. Swartz, D. M. Guldi and A. Hirsch, Supramolecular assembly of a quasi-linear heterofullerene–porphyrin dyad, *J. Mater. Chem.*, 2002, **12**, 2088–2094.

29 J. Marco-Contelles, E. Pérez-Mayoral, A. Samadi, M. d. C. Carreiras and E. Soriano, Recent Advances in the Friedländer Reaction, *Chem. Rev.*, 2009, **109**, 2652–2671.

30 C. J. Tonzola, A. P. Kulkarni, A. P. Gifford, W. Kaminsky and S. A. Jenekhe, Blue-Light-Emitting Oligoquinolines: Synthesis, Properties, and High-Efficiency Blue-Light-Emitting Diodes, *Adv. Funct. Mater.*, 2007, **17**, 863–874.

31 S. P. Economopoulos, A. K. Andreopoulou, V. G. Gregoriou and J. K. Kallitsis, Synthesis and Optical Properties of New End-Functionalized Polyquinolines, *Chem. Mater.*, 2005, **17**, 1063–1071.

32 L. Lu and S. A. Jenekhe, Poly(vinyl diphenylquinoline): A New pH-Tunable Light-Emitting and Charge-Transport Polymer Synthesized by a Simple Modification of Polystyrene, *Macromolecules*, 2001, **34**, 6249–6254.

33 I. Thivaios, S. Kakogianni and G. Bokias, A Library of Quinoline-Labeled Water-Soluble Copolymers with pH-Tunable Fluorescence Response in the Acidic pH Region, *Macromolecules*, 2016, **49**, 3526–3534.

34 S. Yu, S. Wang, H. Yu, Y. Feng, S. Zhang, M. Zhu, H. Yin and X. Meng, A ratiometric two-photon fluorescent probe for hydrazine and its applications, *Sens. Actuators, B*, 2015, **220**, 1338–1345.

35 A. A. Stefopoulos, S. N. Kourkouli, S. Economopoulos, F. Ravani, A. Andreopoulou, K. Papagelis, A. Siokou and J. K. Kallitsis, Polymer and Hybrid Electron Accepting Materials Based on a Semiconducting Perfluorophenylquinoline, *Macromolecules*, 2010, **43**, 4827–4828.

36 L. Sygellou, S. Kakogianni, A. K. Andreopoulou, K. Theodosiou, G. Leftheriotis, J. K. Kallitsis and A. Siokou, Evaluation of the electronic properties of perfluorophenyl functionalized quinolines and their hybrids with carbon nanostructures, *Phys. Chem. Chem. Phys.*, 2016, **18**, 4154–4165.

37 S. Kakogianni, S. N. Kourkouli, A. K. Andreopoulou and J. K. Kallitsis, A versatile approach for creating hybrid semiconducting polymer–fullerene architectures for organic electronics, *J. Mater. Chem. A*, 2014, **2**, 8110–8117.

38 S. Berardi, S. Drouet, L. Francàs, C. Gimbert-Suriñach, M. Guttentag, C. Richmond, T. Stoll and A. Llobet, Molecular artificial photosynthesis, *Chem. Soc. Rev.*, 2014, **43**, 7501–7519.

39 A. N. Webber and W. Lubitz, P700: the primary electron donor of photosystem I, *Biochim. Biophys. Acta, Bioenerg.*, 2001, **1507**, 61–79.

40 M. Rudolf, S. V. Kirner and D. M. Guldi, A multicomponent molecular approach to artificial photosynthesis – the role of fullerenes and endohedral metallofullerenes, *Chem. Soc. Rev.*, 2016, **45**, 612–630.

41 V. Nikolaou, A. Charisiadis, C. Stangel and G. Charalambidis, Porphyrinoid–Fullerene Hybrids as Candidates in Artificial Photosynthetic Schemes, *C*, 2019, **5**, 57.

42 V. Valderrey, G. Aragay and P. Ballester, Porphyrin tweezer receptors: binding studies, conformational properties and applications, *Coord. Chem. Rev.*, 2014, **258–259**, 137–156.

43 M. Davor, Host–guest Studies of Bis-porphyrins, *Curr. Org. Chem.*, 2012, **16**, 829–851.

44 T. Haino, T. Fujii and Y. Fukazawa, Guest Binding and New Self-Assembly of Bisporphyrins, *J. Org. Chem.*, 2006, **71**, 2572–2580.

45 G. Pagona, S. P. Economopoulos, T. Aono, Y. Miyata, H. Shinohara and N. Tagmatarchis, Molecular recognition of La@C82 endohedral metallofullerene by an isophthaloyl-bridged porphyrin dimer, *Tetrahedron Lett.*, 2010, **51**, 5896–5899.

46 D. Sun, F. S. Tham, C. A. Reed, L. Chaker and P. D. W. Boyd, Supramolecular Fullerene-Porphyrin Chemistry. Fullerene

Complexation by Metalated "Jaws Porphyrin" Hosts, *J. Am. Chem. Soc.*, 2002, **124**, 6604–6612.

47 Z.-Y. Xiao, J.-L. Hou, X.-K. Jiang, Z.-T. Li and Z. Ma, Complexes between hydrogen bonded bisporphyrin tweezers and cholesterol-appended fullerenes as organogelators and liquid crystals, *Tetrahedron*, 2009, **65**, 10182–10191.

48 M. Fathalla and J. Jayawickramarajah, Configurational Isomers of a Stilbene-Linked Bis(porphyrin) Tweezer: Synthesis and Fullerene-Binding Studies, *Eur. J. Org. Chem.*, 2009, **2009**, 6095–6099.

49 M. Pérez Emilio and N. Martín, Molecular tweezers for fullerenes, *Pure Appl. Chem.*, 2010, **82**, 523.

50 R. M. K. Calderon, J. Valero, B. Grimm, J. de Mendoza and D. M. Guldi, Enhancing Molecular Recognition in Electron Donor–Acceptor Hybrids *via* Cooperativity, *J. Am. Chem. Soc.*, 2014, **136**, 11436–11443.

51 M. Tanaka, K. Ohkubo, C. P. Gros, R. Guilard and S. Fukuzumi, Persistent Electron-Transfer State of a π-Complex of Acridinium Ion Inserted between Porphyrin Rings of Cofacial Bisporphyrins, *J. Am. Chem. Soc.*, 2006, **128**, 14625–14633.

52 A. Chaudhary and S. P. Rath, Encapsulation of TCNQ and the Acridinium Ion within a Bisporphyrin Cavity: Synthesis, Structure, and Photophysical and HOMO–LUMO-Gap-Mediated Electron-Transfer Properties, *Chem.–Eur. J.*, 2012, **18**, 7404–7417.

53 K. J. Kallitsis, R. Nannou, A. K. Andreopoulou, M. K. Daletou, D. Papaioannou, S. G. Neophytides and J. K. Kallitsis, Crosslinked wholly aromatic polyether membranes based on quinoline derivatives and their application in high temperature polymer electrolyte membrane fuel cells, *J. Power Sources*, 2018, **379**, 144–154.

54 C. M. Cardona, W. Li, A. E. Kaifer, D. Stockdale and G. C. Bazan, Electrochemical Considerations for Determining Absolute Frontier Orbital Energy Levels of Conjugated Polymers for Solar Cell Applications, *Adv. Mater.*, 2011, **23**, 2367–2371.

55 S. Haffner, T. Pichler, M. Knupfer, B. Umlauf, R. Friedlein, M. S. Golden, J. Fink, M. Keshavarz-K, C. Bellavia-Lund, A. Sastre, J. C. Hummelen and F. Wudl, The electronic structure of (C59N)2 from high energy spectroscopy, *Eur. Phys. J. B*, 1998, **1**, 11–17.

56 D. Brynn Hibbert and P. Thordarson, The death of the Job plot, transparency, open science and online tools, uncertainty estimation methods and other developments in supramolecular chemistry data analysis, *Chem. Commun.*, 2016, **52**, 12792–12805.

57 E. W. Driscoll, J. R. Hunt and J. M. Dawlaty, Photobasicity in Quinolines: Origin and Tunability *via* the Substituents' Hammett Parameters, *J. Phys. Chem. Lett.*, 2016, **7**, 2093–2099.

58 S. A. Jenekhe and X. L. Chen, Self-Assembled Aggregates of Rod-Coil Block Copolymers and Their Solubilization and Encapsulation of Fullerenes, *Science*, 1998, **279**, 1903.

59 E. W. Driscoll, J. R. Hunt and J. M. Dawlaty, Proton Capture Dynamics in Quinoline Photobases: Substituent Effect and Involvement of Triplet States, *J. Phys. Chem. A*, 2017, **121**, 7099–7107.

60 S. E. Braslavsky, A. M. Braum, A. E. Cassano, A. V. Emeline, M. I. Litter, L. Palmisano, V. N. Parmon and N. Serpone, Glossary of terms used in photocatalysis and radiation catalysis (IUPAC Recommendations 2011), *Pure Appl. Chem.*, 2011, **83**, 931–1014.

61 M. Fujitsuka, A. Masuhara, H. Kasai, H. Oikawa, H. Nakanishi, O. Ito, T. Yamashiro, Y. Aso and T. Otsubo, Photoinduced Charge Separation and Recombination Processes in Fine Particles of Oligothiophene-C60 Dyad Molecules, *J. Phys. Chem. B*, 2001, **105**, 9930–9934.

62 J. L. Delgado, M. E. El-Khouly, Y. Araki, M. J. Gómez-Escalonilla, P. de la Cruz, F. Oswald, O. Ito and F. Langa, Synthesis and photophysical properties of a [60]fullerene compound with dimethylaniline and ferrocene connected through a pyrazolino group: a study by laser flash photolysis, *Phys. Chem. Chem. Phys.*, 2006, **8**, 4104–4111.